A modular platform to display multiple hemagglutinin subtypes on a single immunogen

Dana Thornlow Lamson[1,2], Faez Amokrane Nait Mohamed[1], Mya Vu[1], Daniel P. Maurer[1,2], Larance Ronsard[1], Daniel Lingwood[1], Aaron G. Schmidt[1,2*]

[1]Ragon Institute of Mass General, MIT, and Harvard, Cambridge, MA, 02139, USA

[2]Department of Microbiology, Harvard Medical School, Boston, MA 02115, USA

Key words: influenza, immunogen design, nanoparticle, vaccine, hemagglutinin, protein engineering

Correspondence:
Aaron G. Schmidt
Tel: 857-268-7118
E-mail: aschmidt@crystal.harvard.edu

ABSTRACT

Next-generation influenza vaccines aim to elicit cross-reactive humoral responses to multiple influenza subtypes. Such increased breadth would not only improve seasonal vaccines but may afford 'universal' protection against influenza subtypes including those with pandemic potential. Here, we describe a "beads-on-a-string" (BOAS) immunogen, that tandemly links up to eight distinct hemagglutinin (HA) head domains from circulating and non-circulating influenzas. These BOAS are immunogenic in the murine model and elicit comparable serum responses to each individual component. Notably, we also find that BOAS elicit cross-reactive, and neutralizing responses to influenza subtypes not included in the immunizing immunogen. Furthermore, BOAS conjugation to protein-based ferritin nanoparticles does not significantly augment serum responses suggesting that our BOAS platform is sufficient for eliciting cross-reactive responses without off-target effects induced by the nanoparticle scaffold. This mix-and-match immunogen design strategy is a robust platform for eliciting responses to multiple influenza subtypes via a single immunogen, and a potential platform for other viral glycoproteins.

INTRODUCTION

Influenza viruses, despite continuous surveillance and annual vaccination, are a significant public health problem resulting in ~500,000 deaths per year[1]. This is largely a consequence of viral evolution as it circulates within animal reservoirs (*e.g.,* avian, swine) and humans and ultimately impacts vaccine effectiveness. To combat this, global surveillance is necessary to inform re-formulation of influenza vaccines to match circulating strains. However, long lead times for vaccine preparation in eggs and mutations acquired during that process[2] can lead to vaccine mismatch and subsequent ineffectiveness. The SARS-CoV-2 pandemic has additionally underscored the need for pandemic preparedness as humans increasingly come into contact with animal reservoirs. Indeed, several avian influenzas, such as H5N1, H7N9 and H9N2, are currently being monitored for their pandemic potential. Thus, there is an urgent need to develop so-called "universal" influenza vaccines that provide protection against both currently circulating (*e.g.,* H1N1s, H3N2s, and Bs) and potentially pandemic viruses.

Several approaches have been taken to improve upon current influenza vaccines, largely focused on the influenza surface glycoprotein, hemagglutinin (HA). A major goal of immunogen design efforts is to elicit antibodies toward conserved epitopes on HA, including the receptor binding site (RBS)[3–9], trimer interface[10–14], and stem[15–20]; antibodies targeting such epitopes are often broadly protective. Indeed, RBS-directed antibodies often are potently neutralizing, as they directly inhibit HA engagement with host cell sialic acid, while interface- and stem-directed antibodies generally protect via Fc-dependent mechanisms (*e.g.,* ADCC, ADCP). Several rational immunogen design approaches[21] such as epitope removal[22,23], domain chimeras[24], computational sequence optimization (COBRAs)[25–29], epitope resurfacing[30] and hyperglycosylation[14,31,32] attempt to focus to these epitopes.

An additional strategy to enrich for cross-reactive antibodies includes increasing antigen valency by displaying multiple antigens on a scaffold, such as a nanoparticle[33–35]. Such multivalency is thought to enhance immunogenicity and antigenicity by spacing antigens near one another in order to effectively cross-link B cell receptors (BCRs)[36]. Ferritin, which can display 24 antigens at its 8 three-fold axes, has been used for influenza, Epstein-Barr virus, coronavirus, and HIV glycoproteins[37–43]. For influenza, following immunization with a mixture of homotypic full-length

seasonal H1, H3, and influenza B HA trimers displayed on ferritin nanoparticles, mice elicited responses with enhanced potency and breadth relative to the trivalent inactivated influenza vaccine (TIV) standard[38]. Based on this success, they then designed "mosaic" ferritin nanoparticles that displayed up to eight antigenically distinct H1 subtype HA receptor binding domains (RBDs) on a single particle, which outperformed admixtures of homotypic nanoparticles and elicited cross-reactive H1 broadly neutralizing antibodies[41]. Further iterations of nanoparticle immunogens have co-displayed multiple full-length HA antigens on virus-like particles (VLPs)[44] and *de novo* designed particles[45], and the latter is currently in clinical trials[45,46,47].

An alternative approach for multivalent display involves tandemly linking antigens into a single polypeptide. This method may alleviate manufacturing challenges related to preparing multiple individual components for mosaic nanoparticles while still increasing size and valency of antigens. For example, using domain III from the dengue envelope surface glycoprotein, a bivalent[48] or quadrivalent[49] tandemly linked immunogen elicited neutralizing antibody responses to all four dengue serotypes and provided protection upon challenge. An analogous approach tandemly linked four different coronavirus RBDs into a single immunogen[50]. These "quartets" elicited responses to each individual components similar to a "mosaic-4" nanoparticle that displayed monomeric RBDs on the surface of a virus like particle (VLP) nanoparticle[46,47]; these approaches were then combined and quartets displaying four or eight unique RBDs were multivalently displayed on VLP nanoparticles. This combinatorial approach augmented both neutralization titers and cross-reactive responses.

Here, we tandemly linked multiple HA subtypes into a single immunogen via short, flexible linkers in a "plug and play" platform we call "beads-on-a-string" or BOAS. These recombinantly produced, protein-based immunogens have between three and eight unique HA heads including circulating and non-circulating A and B influenzas. Mice immunized with either 3, 4, 5, 6, 7, or 8mer BOAS elicited responses to matched and mismatched HA components and could neutralize subsequent replication-restricted reporter (R3) viruses[51]. To further enhance valency, we generated two 4mer BOAS that included 8 different HA heads, conjugated both to ferritin nanoparticles using SpyTag-SpyCatcher[52,53], and showed that the serum responses elicited similar responses to the 8mer. Collectively, these BOAS immunogens could serve as a means to elicit responses to multiple

HA subtypes as a single immunogen and represents a general approach for multivalent display of other viral antigens.

RESULTS

Design and characterization of beads-on-a-string (BOAS)

Monomeric hemagglutinin (HA) heads representing antigenically distinct subtypes were tandemly linked together as a single linear construct, separated by a short, flexible glycine-serine-serine (GSS) linker, which we termed beads-on-a-string (BOAS) immunogens. Eight unique HA subtypes spanning group 1 and 2 influenza A viruses, as well as an influenza B virus, from seasonal, circulating, and non-circulating influenzas were selected to understand the permissibility of the platform to express different HAs (**Figure 1A**). We found that monomeric HA head domains varied in expression levels depending on the boundaries selected: H1, H5, and H7 HA monomers spanned residues 57-261 (H3 numbering), whereas H2, H3, H4, H9, and B HA monomers spanned residues 37-316 (H3 numbering) (**Figure 1B**). We then asked whether we could tandemly link multiple HA heads together as a single construct. Using linkers with either two, three, or four GSS repeats, we tandemly linked representative H1, H3, and B HAs (**Supplemental Figure 1A**) together for recombinant expression in mammalian cells. Each construct, regardless of linker length expressed to similar levels (**Supplemental Figure 1B**) and each individual HA component could be detected with a conformation specific and subtype specific monoclonal antibody (mAb) (**Supplemental Figure 1C**). We next assessed whether order of the HA heads adversely affected expression or accessibility to the conformation-specific mAb. Using H5, H7, and H9 HA heads we created two constructs 1) H5-H9-H7 and 2) H9-H5-H7 each with a four GSS linker. Each construct had comparable levels of expression and reactivity to the respective mAbs (**Supplemental Figure 2**).

Based on these initial data, we next designed six constructs with three to eight individual HA head components from representative H1, H2, H3, H4, H5, H7, H9, and B influenzas; to maximize spacing between each HA component we used the 4x GSS linker. Each BOAS was cloned into a single polypeptide chain with a protease-cleavable C-terminal purification tag (**Figure 1C**). We

synthesized six different BOAS, and define each construct as 3mer, 4mer, etc., referencing the number of HA components (**Figure 1D**). Each BOAS construct could be purified to homogeneity as assayed by SDS-PAGE after immobilized metal affinity chromatography (**Figure 2A**) and correspond to the expected molecular weight following proteolytic cleavage of native glycans with PNGase-F (**Figure 2B**). After size-exclusion chromatography (SEC), the non-PNGase-treated BOAS were monodispersed (**Figure 2C**).

We then analyzed the BOAS using negative stain electron microscopy (NS-EM). Individual HAs were readily discernable and equal to the number of components in the respective BOAS (**Figure 2D and 2E**); we observed that the 3mer could adopt both extended and collapsed, triangular-like conformations (**Figure 2D**), whereas longer BOAS, such as the 8mer, adopted a rosette-like conformation (**Figure 2E**). This is likely a consequence of the flexible GSS linker separating the individual HA head components.

To assess conformational integrity and ensure that each HA present was properly folded, we assembled a panel of conformation- and subtype-specific mAbs to assay each individual component. This included mAb S5V2-29[12] a broadly-reactive interface-directed positive control antibody and mAbs 5J8[4,6], 2G1[5], K03.12[55], P2-D9 (**Supplemental Figure 3**), H5.3[56], H7.167[57], and H1209[58] which are specific to H1, H2, H3, H5, H5, H7 and B subtypes, respectively; an H9 conformation-specific mAb was not available. Each individual HA component was detected using subtype-specific mAb in ELISA, and overall affinity for each component was comparable regardless of BOAS length (**Figure 2F**). Collectively, these data support a plug-and-play platform that can readily exchange HA components while retaining conformational integrity.

Immunogenicity of BOAS

To determine immunogenicity of each BOAS, we performed a prime-boost-boost vaccination regimen in C5BL/6 mice at two-week intervals (**Figure 3A**) and tested serum reactivity to both BOAS immunogen as well as individual full-length HA trimers of each component. Serum titers against the immunogen were detectable after a single prime, and increased following a boost, and stayed relatively level until day 42 (**Figure 3B**). Serum responses varied for differing BOAS lengths, with the 4mer and 5mer BOAS being the most immunogenic (**Figure 3C**). BOAS-elicited

serum, regardless of its length, reacted to full-length HAs representing individual components (**Figure 3D**). For example, the 6mer, which contains heads of H1, H2, H3, H4, H5, and H7, showed reactivity to full length matched HAs. Interestingly, some BOAS elicited cross-reactivity to mis-matched components not present in the immunogen. For example, the 3mer, which contained H1, H2, and H3 HA heads, elicited detectable titers to an H4 HA, and the 5mer, which contained H1, H2, H3, H4, and H5 HA heads, had detectable titers to H7 (**Figure 3D**).

Cross-reactivity of immune responses

To understand potential cross-reactivity observed in the serum analyses, across we used a Consurf-like[59,60] method to assess sequence conservation across the eight HA components in the BOAS. Each component of the BOAS was aligned structurally to the H2 head domain and scored at each position for their amino acid conservation at each position on a scale of 1 to 9. These were then pseudo-colored on the structure to visualize conserved and variable epitopes across the head domain surface (**Figure 4A**). We observed regions of both significant variability as well as conservation, notably the trimer interface (TI), as well as the core sialic acid interacting residues in the receptor binding site (RBS), the latter which remained nearly 100% conserved in all BOAS (**Figure 4A**). This was quantitated by taking the average amino acid (AA) conservation score across both the RBS and interface epitopes as well as the entire sequence, and we see that these epitopes retain higher conservation relative to the overall sequence as BOAS length increases. We then determined approximate degrees of focusing to the TI and RBS via a serum competition ELISA using mAbs. All the BOAS maintained, approximately, between 15-35% focusing to the TI epitope, whereas focusing the RBS was more variable (**Figure 4C**). Both RBS focusing (**Figure 4D**) and TI focusing (**Figure 4E**) trended similarly with homology scores for each epitope, indicating epitope conservation may be influencing immune focusing to particular epitopes.

Design of BOAS-conjugated nanoparticles

To further increase avidity affects as well as potential immunogenicity, we split our 8mer BOAS into two 4mer BOAS and attached both in an equal molar ratio to *H. pylori* ferritin nanoparticles (NPs) using SpyTag-SpyCatcher[52], herein referred to as BOAS-NPs (**Figure 5A**). The two 4mer BOAS efficiently conjugated to nanoparticles as determined by SEC and SDS-PAGE (**Supplemental Figure 4**), Further biophysical characterization using dynamic light scattering

(DLS) showed a shift of from 9.8 ± 1.1 nm to 21.3 ± 2.0 nm and NS-EM showed spherical particles with projections. (**Figure 5D and 5E**). We verified the presence and structural integrity of each BOAS component on the nanoparticles using an ELISA with the same panel of conformation and subtype-specific mAbs, (**Figure 5E**).

Immunogenicity of BOAS-conjugated nanoparticles

We next immunized mice with BOAS-NP and a SpyCatcher NP control to assess immunogenicity. Mice were immunized with an equal amount of NP relative to the BOAS (20µg), in an equivalent homologous prime-boost-boost regimen (**Figure 6A**). The BOAS-NP was significantly more immunogenic than the SpyCatcher NP control, eliciting titers approximately an order of magnitude greater by d42 (**Figure 6B**). The BOAS NP, however, elicited significantly reduced titers to the SpyCatcher NP scaffold relative to the control (**Figure 6C**). When each group was evaluated for titers against both the BOAS components, the SpyCatcher nanoparticle scaffold, or BOAS-NP (**Figure 6D,E**), the BOAS-NP elicited equivalent titers to each set of BOAS, and greater titers to the decorated nanoparticle relative to the ferritin scaffold (**Figure 6E**). When we examined titers to individual HA components, we observed detectable titers over baseline to all eight HAs present on the BOAS-NPs (**Figure 6F**). When compared to the immunogenicity of the 3mer to 8mer BOAS immunogens, the BOAS-NP showed comparable titers to each component relative to BOAS that contained a given component (**Figure 6H**).

Neutralization of influenza viruses by BOAS-elicited sera

We next determined serum neutralization titers to matched and mis-matched influenza viruses based on the BOAS components (**Figure 7**). We tested serum from mice immunized with all BOAS against H1/Michigan/2015 and H3/Kansas/2017 virus, whose HA was present in all the BOAS. These showed varying neutralization titers to both viruses, with all matched BOAS neutralizing virus except for the 8mer and H1N1 virus. Additionally, we tested serum against H7/Shanghai/2013 virus, which was present in the 6mer, 7mer, 8mer, and BOAS-conjugated nanoparticle; all matched BOAS neutralized H7 virus. Of the mismatched viruses, only the 5mer also strongly neutralized H7 virus. Finally, we tested neutralization titers to H5N1 virus. However, only the BOAS-NP serum neutralized this virus, despite the component being present in the other BOAS tested. Serum from the BOAS-conjugated nanoparticle group elicited neutralization titers

to all four viruses though at varying degrees relative to the BOAS alone. This neutralization was dependent on the presence of BOAS, as the scaffold control serum did not neutralize any viruses tested.

DISCUSSION

Here we engineered "beads-on-a-string" (BOAS) that included tandemly linked, antigenically distinct HA heads as a single construct. This platform allows a mixing-and-matching of up to eight distinct HA heads from both influenza A and B viruses. Furthermore, we showed that the order and number of HA heads can vary without losing reactivity to conformation-specific mAbs *in vitro*, highlighting the flexibility of this platform. Mice immunized with BOAS had comparable serum reactivity to each individual component; though relative binding and neutralization titers varied between immunogens; this is likely a consequence of length and/or composition. Further oligomerization for increased multivalent display was accomplished by conjugating two 4mer BOAS inclusive of eight distinct HA heads to a ferritin nanoparticle via SpyTag/SpyCatcher ligation. Similar to the BOAS, these conjugated nanoparticles elicited similar titers to all eight HA components and could neutralize matched viruses.

Thus, tandemly linking HA heads is a robust method for displaying multiple influenza subtypes in a single protein-based immunogen. Binding titers were elicited to all components present in the immunogen, and there was no significant correlation between HA position within the BOAS (*i.e.,* terminal or internal) and immunogenicity. However, relative immunogenicities of each HA varied despite the guaranteed equimolar display of each subtype. There were qualitatively immunodominant HAs, notably H4 and H9, and these were relatively consistent across BOAS in which they were a component. Further studies using the modularity of the BOAS could further deconvolute relative immunodominances of HA subtypes.

Despite similar binding titers across multiple BOAS lengths, expression levels and neutralization titers were quite variable. While all 3mer to 8mer BOAS could be overexpressed, expression inversely correlated with overall length. To mitigate this, multiple BOAS (*e.g.,* two 4mers) or conjugation to protein-based nanoparticles, as was done here, could be used to ensure coverage of each desired HA subtype. Furthermore, neutralization titers were quite variable across different

BOAS lengths despite similar binding titers. This may be related to multiple factors including homology, stability, and accessibility of neutralizing epitopes for different BOAS lengths. Studies manipulating BOAS composition at intermediate lengths could optimize neutralizing responses to particular influenzas of interest.

Based on the immunogenicity of the various BOAS and their ability to elicit neutralizing responses, it may not be necessary to maximize the number of HA heads into a single immunogen. Indeed, it qualitatively appears that the 4mer and 5mer BOAS were the most immunogenic and this length may be sufficient to effectively engage and crosslink BCR for potent stimulation. Furthermore, the 5mer elicited cross-reactive and neutralizing responses to an H7 HA, a mis-matched HA that was not present in the immunogen. Similarly, the 3mer BOAS, which does not contain an H4 component, also elicited detectable titers to the H4 HA. This observed cross-reactivity is likely due to sequence conservation between the HAs, as H3 and H4 share ~51% sequence identity (**Supplemental Figure 5**). However, total sequence homology alone is not sufficient to explain this phenomena, as the 3mer elicited low titers to H5 despite sharing ~46% and ~62% overall sequence identity with H1 and H2, respectively.

Potential enrichment of antibodies targeting the conserved RBS and trimer interface epitopes may also be contributing to observed cross-reactivity. Both epitopes are relatively conserved across all BOAS lengths (**Figure 4C**), and the two BOAS showing the most cross-reactivity, the 3mer and 5mer, elicit a significant portion of the serum response toward both RBS and interface epitopes as determined via a serum competition assay with available epitope-directed antibodies (**Figure 4B**). Isolated interface-directed antibodies, in particular, can engage more than nine unique subtypes across both group 1 and 2 influenzas[10,12], and our monomeric head-based BOAS immunogens, have the otherwise occluded trimer interface epitope exposed[10–12]. Furthermore, we have previously shown that this trimer interface epitope, when exposed, is immunodominant in the murine model[14]. Further studies with different combinations of HAs could aid in understanding how length and composition influences epitope focusing. Combining the BOAS platform with other immune-focusing approaches[32] such as hyperglycosylation[14,31,61,62] or resurfacing[30,63] could enhance cross-reactive responses Additionally, modifying linker spacing and rigidity can also be

used as a mechanism to enhance BCR cross-linking and thus enhance cross-reactive B cell activation and elicitation[64].

BOAS can be further multimerized via conjugation to a surface of a nanoparticle. Interestingly, this only had a marginal effect on immunogenicity. The BOAS conjugated-nanoparticle elicited titers of ~10^4 (**Figure 6B**), whereas the best BOAS alone reached an order of magnitude greater (**Fig 3C**). This appears in contrast with other studies where attaching an antigen to a nanoparticle scaffold enhanced immunogenicity and neutralization potency. One recent example designed quartets of antigenically distinct SARS-like betacoronavirus RBDs coupled to an mi3-VLP scaffold via a similar SpyCatchter/SpyTag system and showed increased binding and neutralization titers following conjugation to the NP compared to quartet alone. This discrepancy may be in part due to the larger mi3 nanoparticle which displays 60 copies of the antigen rather than the 24 copies displayed on the ferritin nanoparticle used in this study. Nevertheless, HA-specific responses were similar whether the BOAS were conjugated to the nanoparticle or not, indicating that HA proximity to the NP surface did not impact responses to each component. This observation is consistent with betacoronavirus quartet nanoparticles as well. Additionally, BOAS conjugation to the nanoparticle significantly reduced the scaffold-directed response to near baseline. The addition of the large BOAS projections to the surface of the nanoparticle likely masked the immunogenic scaffold epitopes[65].

Collectively, this study demonstrates the versatility of the BOAS platform to present multiple HA subtypes as a single immunogen. This "plug-and-play" approach can readily exchange HAs to elicit desired immune responses. BOAS are potentially advantageous over other multivalent display platforms such as protein-based nanoparticles, which can produce off-target responses due to their inherent immunogenicity[38]. Furthermore, when genetic fusions of the antigen to nanoparticles is not possible, SpyCatcher/SpyTag (or another suitable conjugation approach) must be used, further contributing to scaffold-specific responses as well as additional multi-step manufacturing and purification challenges. Not only does our BOAS platform circumvent these potential caveats, but because this is a single polypeptide chain, this immunogen could readily be formulated as an mRNA lipid nanoparticle (LNP)[66]. The BOAS platform forms the basis for next-generation influenza vaccines and can more broadly be readily adapted to other viral antigens.

MATERIALS AND METHODS

Beads-on-a-string (BOAS) immunogen and full-length hemagglutinin (HA) expression and purification

Hemagglutinin (HA) head for BOAS immunogens were designed based on the following sequences from the following subtypes: H1 (H1/A/Michigan/45/2015) (GenBank: AMA11475.1) , H2 (H2/A/Japan/305/1957) (GenBank: AAA43185), H3 (H3/A/Kansas/14/2017) (GenBank: AVG71503), H4 (H4/A/American Black Duck/New Brunswick/00464/2010) (GenBank: AGG81749), H5 (H5/A/Viet Nam/1203/2004) (GenBank: ADD97095), H7 (H7/A/Shanghai/01/2014) (GenBank: AHK10800), H9 (H9/A/Guangdong/MZ058/2016) (GenBank: AOR17625.1), and B (B/Malaysia/2506/2004) (GenBank: ABU99194). Sequences were codon optimized using IDT and subcloned into pVRC vectors for expression in mammalian cells. For BOAS immunogens, all HA heads were separated by a "GA$(GSS)_4$AS" spacer. Specific head domain regions for each subtype were selected based on expression levels in expi293F cells. All protein sequences contained a C-terminal 8x-His tag for purification with an upstream 3C-protease cleavage site. Full-length HA trimers contained an additional C-terminal foldon (Fd) trimerization domain for expression as soluble trimers. BOAS immunogens and HA trimers were transfected in expi293F cells using Expifectamine transfection reagent and enhancers based on manufacturer's instructions. Five days post-transfection, supernatant was harvested and clarified via centrifugation, then purified on a TALON cobalt resin via the 8x-His Tag. Following elution, proteins were then purified on a Superdex 200 (S200) Increase 10/300 GL (for trimeric HAs) or Superose 6 Increase 10/300 GL (for BOAS) size-exclusion column in Dulbecco's Phosphate Buffered Saline (DPBS). Pooled fractions of BOAS were then treated with HRV-3C protease to remove tags for 16 hours at 4°C, then passed over a TALON cobalt resin to remove any remaining protease, cleaved tags, and uncleaved protein. Trimeric HAs were used for ELISAs with purification tags present.

IgG expression and purification

All antibody variable regions were codon optimized for mammalian cell expression and subcloned into pVRC vectors containing either heavy or light (kappa or lambda) with humanized constant regions. Equimolar heavy and light chain plasmids were co-transfected into HEK293F cells using polyethylenimine (PEI). Five days following transfection, supernatants were harvested, clarified

via centrifugation, and purified on a Protein G resin. Purified antibodies were then buffer exchanged into DPBS for use in ELISA assays.

Nanoparticle Assembly

C-terminally SpyTagged BOAS and N-terminal SpyCatcher nanoparticles were subcloned into pVRC expression vectors, then expressed in expi293F cells and purified via TALON cobalt resin as above. SpyTagged BOAS were further purified via size-exclusion chromatography on a Superose 6 column, as above, followed by cleavage of the C-terminal His tag via 3C HRV protease to yield a C-terminal SpyTag. SpyCatcher nanoparticles were purified on a HiPrep Sephacryl S400 column in DPBS. Purified SpyCatcher nanoparticles was when mixed with an equimolar ratio mixture of each 4mer BOAS (H1, H2, H3, H4 and H5, H7, H9,B) at a 1.2 molar excess relative to the nanoparticle overnight at 4°C. The mixture was then re-purified over an S400 column, concentrated, aliquoted, and snap-frozen in liquid nitrogen until use.

Negative Staining procedure for TEM

5µl of the sample was adsorbed for 1 minute onto a carbon-coated grid made hydrophilic by a 20 second exposure to a glow discharge (25mA). Excess liquid was removed with filterpaper (Whatman #1), the grid was then floated briefly on a drop of water (to wash away phosphate or salt), blotted again on a filer paper and then stained with 0.75% uranyl formate or 1% uranyl acetate for 20-30 seconds. After removing the excess stain with a filter paper the grids were examined in a JEOL 1200EX Transmission electron microscope or a TecnaiG² Spirit BioTWIN and images were recorded with an AMT 2k CCD camera.

Immunizations

C57BL/6 mice (Jackson Laboratory) (n=3 per group) were immunized with 20µg of BOAS immunogens of varying length and adjuvanted with 50% Sigmas Adjuvant for a total of 100µL of inoculum. Immunogens and adjuvant were administered intramuscularly (IM) at day 0, day 14, and day 28. Serum samples were collected at days 0, 14, 28, and 42 (prior to immunogen administration). All experiments were conducted in 6-10 week old female mice under the institutional IACUC protocol (2014N000252).

Serum ELISAs

High-binding 96-well plates (Corning) were coated with 200ng per well of BOAS immunogen, nanoparticle, or trimeric HAs overnight at 4°C in DPBS. The following day, plates were blocked with 1% BSA in PBS-T (DPBS+0.1% Tween-20) for 1 hour at RT, rocking. Diluted serum in DPBS were generated starting at a 1:50 dilution, followed by 10-fold serial dilutions for a total of 7 dilutions. After one hour, blocking buffer was discarded, and 40µL of diluted serum was added and incubated for 1 hour at RT, rocking. Serum was then discarded, and plates were washed 3 times with PBS-T, after which 100µL of HRP-conjugated anti-mouse secondary antibody (Abcam) at a 1:20,000 dilution was added and incubated for 1 hour at RT rocking. Following secondary antibody incubation, plates were again washed 3 times with PBS-T. Slow TMB development solution was then added to plates and incubated for 30-40 mins at RT, then stopped with an equal volume of 0.2M sulfuric acid stop solution. Developed plates were then analyzed via absorbance measurements at 450nm. Each condition was blank subtracted with a secondary only control and plotted in GraphPad Prism 10 (v10.0.2). Serum titers were determined using a non-linear regression (Sigmoidal, 4PL, where x is concentration) to determine the dilution at which absorbance is at half maximum. Titers for individual mice against respective antigens were then reported as the inverse of dilution factor at half maximum.

Serum Competition ELISAs

Serum competition ELISAs were performed following a similar protocol to serum ELISAs described above. Following blocking with BSA in PBS-T, blocking solution was discarded and 40µL of either DPBS (no competition control), a cocktail of humanized RBS-directed antibodies (5J8, 2G1, 3E5, P2-D9, H5.3, H7.167, H1209), a cocktail of humanized interface-directed antibodies (S5V2-29, D1 H1-17/H3-14, D2 H1-1/H3-1), or a negative control antibody (MEDI8852) were added at a concentration of 100µg/mL per antibody. Plates were incubated with competing antibodies or controls for 1 hour at RT. Serum from mice from respective BOAS cohorts were diluted by 1:5,000 (3mer and 6mer) or 1:10,000 (4mer, 5mer, 7mer, and 8mer) in DPBS, then 40µL added on top of competing antibody for a final dilution of 1:10,000 (3mer and 6mer) or 1:20,000 (4mer, 5mer, 7mer, and 8mer). These dilutions were selected based on a dilution range in serum ELISAs in which serum reactivity behaved linearly. Plates were incubated with serum and competing antibodies for an additional 1 hour at RT, washed 3 times with PBS-T, then

incubated with an HRP-conjugated human/bovine/horse cross-adsorbed anti-mouse secondary antibody (Southern Biotech) at a 1:20,000 dilution for 1 hour at RT. The remaining wash and development steps were performed as in the serum ELISA.

Microneutralization Assays

Serum microneutralization assays using R3 viruses followed the published protocol in Creanga et al[51]. Briefly, MDCK-SIAT1-PB1/H5/H7 cells were thawed into D10 media with penicillin and streptomycin (P/S) and 10% heat-inactivated fetal bovine serum (FBS) three days prior to infection. Cells were seeded two days later at $1.5x10^4$ cells/well in flu media (Opti-MEM + 0.01% FBS + P/S + 0.3% Bovine Serum Albumin (BSA) + Ca/Mg) overnight at 37°C. Serum was also treated with receptor destroying enzyme (RDE) II at a 1:3 dilution overnight at 37°C, followed by inactivation at 56°C for 30-60 mins. Treated serum was then diluted in media at 1:3 for a final starting dilution of 1:18. On the day of infection, cells were treated with 60µL of virus in flu media + TPCK-trypsin for 1 hour at 37°C with 5% CO_2. After one hour, media was removed via aspiration and cells were treated with 100µL treated serum. The following day, fluorescent foci were counted on a Zeiss Celldiscoverer 7 + LSM900 + Airyscan 2 (CD7+LSM900) to determine neutralization. Counts were normalized to a cell control and untreated virus control, and IC50 values for neutralization were determined via a fit to a 4PL non-linear regression in technical duplicate in Prism v10.0.2 (GraphPad).

Homology Analyses

Homology analyses on HA BOAS was conducted using a manual method analogous to Consurf[59,60]. HA head domain structures (or closely related variants) were aligned in Pymol to the H2 JP-57 structure (PDB: 2WRE). Structures used for alignments were as follows: H1 (PDB: 6XGC), H3 (PDB: 4O5N), H4 (PDB: 5XL3), H5 (PDB: 6CFG), H7 (PDB: 6FYU), H9 (PDB: 1JSI), B (PDB: 4FQJ). Any mis-matches in specific amino acids were adjusted using the mutagenesis wizard in Pymol. Following structural alignment, each position on the HA head domain was scored for % aa identity at each position on a scale of 1-9, where 1 = 10-19% identical, 2 = 20-29% identical … to 9 = 90-100% identical, which we refer to as a "conservation score". This was repeated for each composition of BOAS (i.e. 3mer, 4mer, 5mer, … 8mer). Each position on the H2 structure was then pseudo colored based on the conservation score. Average amino acid

conservation scores were defined as the average of conservation score over the whole sequence (overall), or of amino acids within a given epitope. Interface epitope amino acids were defined as residues 60, 86-106, and 212-232 (H1 numbering), and RBS epitope amino acids were defined as residues 94-96, 128-146, 153-161, 182-194, and 222-229 (H1 numbering).

ACKNOWLEDGMENTS

We thank the mouse facility at the Ragon Institute for mouse maintenance. We also thank Nicholas Lamson for helping with DLS measurements for nanoparticle characterization. We would like to also thank Maria Ericcson for acquiring NS-EM images. We acknowledge support from R01 AI146779 and P01 AI089618 (AGS) and R01AI137057, R01AI153098, and R01AI155447 (DL). This research has been funded in whole or part with federal funds under a contract from the National Institute of Allergy and Infectious Diseases, NIH contract 75N93019C00050 (AGS).

AUTHOR INFORMATION

Author Contributions DTL and AGS designed research; DTL, FAMN, MLV, DPM, and LR performed research; DTL and AGS analyzed data; DTL and AGS wrote the paper. All authors edited and commented on the paper.

Correspondence and requests for materials should be addressed to: Aaron G. Schmidt (aschmidt@crystal.harvard.edu)

Competing financial interest: DTL and AGS have filed a provisional patent covering the work described here.

REFERENCES

1. Wei, C.-J. *et al.* Next-generation influenza vaccines: opportunities and challenges. *Nat Rev Drug Discov* **19**, 239–252 (2020).

2. Raymond, D. D. *et al.* Influenza immunization elicits antibodies specific for an egg-adapted vaccine strain. *Nature Medicine* **22**, 1465–1469 (2016).

3. Ekiert, D. C. *et al.* Cross-neutralization of influenza A viruses mediated by a single antibody loop. *Nature* **489**, 526–532 (2012).

4. Hong, M. *et al.* Antibody recognition of the pandemic H1N1 Influenza virus hemagglutinin receptor binding site. *Journal of Virology* **87**, 12471–12480 (2013).

5. Krause, J. C. *et al.* Human Monoclonal Antibodies to Pandemic 1957 H2N2 and Pandemic 1968 H3N2 Influenza Viruses. *J. Virol.* **86**, 6334–6340 (2012).

6. Krause, J. C. *et al.* A broadly neutralizing human monoclonal antibody that recognizes a conserved, novel epitope on the globular head of the influenza H1N1 virus hemagglutinin. *Journal of Virology* **85**, 10905–10908 (2011).

7. Lee, P. S. *et al.* Receptor mimicry by antibody F045-092 facilitates universal binding to the H3 subtype of influenza virus. *Nature Communications* **5**, 3614–9 (2014).

8. Lee, P. S. *et al.* Heterosubtypic antibody recognition of the influenza virus hemagglutinin receptor binding site enhanced by avidity. *Proc National Acad Sci* **109**, 17040–17045 (2012).

9. Schmidt, A. G. *et al.* Preconfiguration of the antigen-binding site during affinity maturation of a broadly neutralizing influenza virus antibody. *Proceedings of the National Academy of Sciences of the United States of America* **110**, 264–269 (2013).

10. McCarthy, K. R. *et al.* A Prevalent Focused Human Antibody Response to the Influenza Virus Hemagglutinin Head Interface. *Mbio* **12**, e01144-21 (2021).

11. Bangaru, S. *et al.* A Site of Vulnerability on the Influenza Virus Hemagglutinin Head Domain Trimer Interface. *Cell* **177**, 1136-1152.e18 (2019).

12. Watanabe, A. *et al.* Antibodies to a Conserved Influenza Head Interface Epitope Protect by an IgG Subtype-Dependent Mechanism. *Cell* **177**, 1124-1135.e16 (2019).

13. Dong, J. *et al.* Anti–influenza H7 human antibody targets antigenic site in hemagglutinin head domain interface. *J Clin Invest* **130**, 4734–4739 (2020).

14. Bajic, G. *et al.* Influenza Antigen Engineering Focuses Immune Responses to a Subdominant but Broadly Protective Viral Epitope. *Cell Host Microbe* **25**, 827-835.e6 (2019).

15. Corti, D. *et al.* A Neutralizing Antibody Selected from Plasma Cells that Binds to Group 1 and Group 2 Influenza A Hemagglutinins. *Science* **333**, 850–856 (2011).

16. Dreyfus, C., Ekiert, D. C. & Wilson, I. A. Structure of a classical broadly neutralizing stem antibody in complex with a pandemic H2 influenza virus hemagglutinin. *Journal of Virology* **87**, 7149–7154 (2013).

17. Dreyfus, C. *et al.* Highly conserved protective epitopes on influenza B viruses. *Science* **337**, 1343–1348 (2012).

18. Ekiert, D. C. *et al.* Antibody Recognition of a Highly Conserved Influenza Virus Epitope. *Science* **324**, 246–251 (2009).

19. Friesen, R. H. E. *et al.* A common solution to group 2 influenza virus neutralization. *Proc. Natl. Acad. Sci.* **111**, 445–450 (2014).

20. Kallewaard, N. L. *et al.* Structure and Function Analysis of an Antibody Recognizing All Influenza A Subtypes. *Cell* **166**, 596–608 (2016).

21. Caradonna, T. M. & Schmidt, A. G. Protein engineering strategies for rational immunogen design. *Npj Vaccines* **6**, 154 (2021).

22. Impagliazzo, A. *et al.* A stable trimeric influenza hemagglutinin stem as a broadly protective immunogen. *Science* **349**, 1301–1306 (2015).

23. Yassine, H. M. *et al.* Hemagglutinin-stem nanoparticles generate heterosubtypic influenza protection. *Nature Medicine* **21**, 1065–1070 (2015).

24. Nachbagauer, R. *et al.* A chimeric hemagglutinin-based universal influenza virus vaccine approach induces broad and long-lasting immunity in a randomized, placebo-controlled phase I trial. *Nature Medicine* 1–20 (2020) doi:10.1038/s41591-020-1118-7.

25. Giles, B. M. & Ross, T. M. A computationally optimized broadly reactive antigen (COBRA) based H5N1 VLP vaccine elicits broadly reactive antibodies in mice and ferrets. *Vaccine* **29**, 3043–3054 (2011).

26. Skarlupka, A. L., Reneer, Z. B., Abreu, R. B., Ross, T. M. & Sautto, G. A. An Influenza Virus Hemagglutinin Computationally Optimized Broadly Reactive Antigen Elicits Antibodies Endowed with Group 1 Heterosubtypic Breadth against Swine Influenza Viruses. *J. Virol.* **94**, (2020).

27. Reneer, Z. B., Jamieson, P. J., Skarlupka, A. L., Huang, Y. & Ross, T. M. Computationally Optimized Broadly Reactive H2 HA Influenza Vaccines Elicited Broadly Cross-Reactive Antibodies and Protected Mice from Viral Challenges. *J. Virol.* **95**, (2020).

28. Wong, T. M. *et al.* Computationally Optimized Broadly Reactive Hemagglutinin Elicits Hemagglutination Inhibition Antibodies against a Panel of H3N2 Influenza Virus Cocirculating Variants. *J. Virol.* **91**, (2017).

29. Carter, D. M. *et al.* Design and Characterization of a Computationally Optimized Broadly Reactive Hemagglutinin Vaccine for H1N1 Influenza Viruses. *J. Virol.* **90**, 4720–4734 (2016).

30. Bajic, G. *et al.* Structure-Guided Molecular Grafting of a Complex Broadly Neutralizing Viral Epitope. *Acs Infect Dis* **6**, 1182–1191 (2020).

31. Thornlow, D. N. *et al.* Altering the Immunogenicity of Hemagglutinin Immunogens by Hyperglycosylation and Disulfide Stabilization. *Front Immunol* **12**, 737973 (2021).

32. Dosey, A. *et al.* Combinatorial immune refocusing within the influenza hemagglutinin head elicits cross-neutralizing antibody responses. *bioRxiv* 2023.05.23.541996 (2023) doi:10.1101/2023.05.23.541996.

33. Bachmann, M. F. & Jennings, G. T. Vaccine delivery: a matter of size, geometry, kinetics and molecular patterns. *Nat. Rev. Immunol.* **10**, 787–796 (2010).

34. Nguyen, B. & Tolia, N. H. Protein-based antigen presentation platforms for nanoparticle vaccines. *npj Vaccines* **6**, 70 (2021).

35. Curley, S. M. & Putnam, D. Biological Nanoparticles in Vaccine Development. *Front. Bioeng. Biotechnol.* **10**, 867119 (2022).

36. Bachmann, M. F. & Jennings, G. T. Vaccine delivery: a matter of size, geometry, kinetics and molecular patterns. *Nat. Rev. Immunol.* **10**, 787–796 (2010).

37. Joyce, M. G. *et al.* A SARS-CoV-2 ferritin nanoparticle vaccine elicits protective immune responses in nonhuman primates. *Sci. Transl. Med.* **14**, eabi5735 (2021).

38. Kanekiyo, M. *et al.* Self-assembling influenza nanoparticle vaccines elicit broadly neutralizing H1N1 antibodies. *Nature* **498**, 102–106 (2013).

39. Georgiev, I. S. *et al.* Two-Component Ferritin Nanoparticles for Multimerization of Diverse Trimeric Antigens. *ACS Infectious Diseases* **4**, 788–796 (2018).

40. He, L. *et al.* Presenting native-like trimeric HIV-1 antigens with self-assembling nanoparticles. *Nat. Commun.* **7**, 12041 (2016).

41. Kanekiyo, M. *et al.* Mosaic nanoparticle display of diverse influenza virus hemagglutinins elicits broad B cell responses. *Nature Immunology* 1–18 (2019) doi:10.1038/s41590-018-0305-x.

42. McLeod, B. *et al.* Vaccination with a structure-based stabilized version of malarial antigen Pfs48/45 elicits ultra-potent transmission-blocking antibody responses. *Immunity* (2022) doi:10.1016/j.immuni.2022.07.015.

43. Kanekiyo, M. *et al.* Rational Design of an Epstein-Barr Virus Vaccine Targeting the Receptor-Binding Site. *Cell* **162**, 1090–1100 (2015).

44. Cohen, A. A. *et al.* Construction, characterization, and immunization of nanoparticles that display a diverse array of influenza HA trimers. *Plos One* **16**, e0247963 (2021).

45. Boyoglu-Barnum, S. *et al.* Quadrivalent influenza nanoparticle vaccines induce broad protection. *Nature* 1–6 (2021) doi:10.1038/s41586-021-03365-x.

46. Cohen, A. A. *et al.* Mosaic RBD nanoparticles protect against challenge by diverse sarbecoviruses in animal models. *Science* (2022) doi:10.1126/science.abq0839.

47. Cohen, A. A. *et al.* Mosaic nanoparticles elicit cross-reactive immune responses to zoonotic coronaviruses in mice. *Sci New York N Y* **371**, 735–741 (2021).

48. Zhao, H. *et al.* Induction of Neutralizing Antibodies against Four Serotypes of Dengue Viruses by MixBiEDIII, a Tetravalent Dengue Vaccine. *PLoS ONE* **9**, e86573 (2014).

49. Etemad, B. *et al.* An envelope domain III-based chimeric antigen produced in Pichia pastoris elicits neutralizing antibodies against all four dengue virus serotypes. *Am. J. Trop. Med. Hyg.* **79**, 353–63 (2008).

50. Hills, R. A. *et al.* Multiviral Quartet Nanocages Elicit Broad Anti-Coronavirus Responses for Proactive Vaccinology. *bioRxiv* 2023.02.24.529520 (2023) doi:10.1101/2023.02.24.529520.

51. Creanga, A. *et al.* A comprehensive influenza reporter virus panel for high-throughput deep profiling of neutralizing antibodies. *Nat Commun* **12**, 1722 (2021).

52. Zakeri, B. *et al.* Peptide tag forming a rapid covalent bond to a protein, through engineering a bacterial adhesin. *Proc. Natl. Acad. Sci.* **109**, E690–E697 (2012).

53. Sutherland, A. R., Alam, Md. K. & Geyer, C. R. Post-translational Assembly of Protein Parts into Complex Devices by Using SpyTag/SpyCatcher Protein Ligase. *ChemBioChem* **20**, 319–328 (2019).

54. Ainavarapu, S. R. K. *et al.* Contour Length and Refolding Rate of a Small Protein Controlled by Engineered Disulfide Bonds. *Biophys. J.* **92**, 225–233 (2007).

55. McCarthy, K. R. *et al.* Memory B Cells that Cross-React with Group 1 and Group 2 Influenza A Viruses Are Abundant in Adult Human Repertoires. *Immunity* **48**, 174-183.e9 (2018).

56. Winarski, K. L. *et al.* Vaccine-elicited antibody that neutralizes H5N1 influenza and variants binds the receptor site and polymorphic sites. *Proceedings of the National Academy of Sciences of the United States of America* **112**, 9346–9351 (2015).

57. Thornburg, N. J. *et al.* H7N9 influenza virus neutralizing antibodies that possess few somatic mutations. *J Clin Invest* **126**, 1482–1494 (2016).

58. Bajic, G. & Harrison, S. C. Antibodies That Engage the Hemagglutinin Receptor-Binding Site of Influenza B Viruses. *Acs Infect Dis* **7**, 1–5 (2020).

59. Glaser, F. *et al.* ConSurf: Identification of Functional Regions in Proteins by Surface-Mapping of Phylogenetic Information. *Bioinformatics* **19**, 163–164 (2003).

60. Ashkenazy, H. *et al.* ConSurf 2016: an improved methodology to estimate and visualize evolutionary conservation in macromolecules. *Nucleic Acids Res.* **44**, W344–W350 (2016).

61. Ingale, J. *et al.* Hyperglycosylated Stable Core Immunogens Designed To Present the CD4 Binding Site Are Preferentially Recognized by Broadly Neutralizing Antibodies. *J Virol* **88**, 14002–14016 (2014).

62. Eggink, D., Goff, P. H. & Palese, P. Guiding the Immune Response against Influenza Virus Hemagglutinin toward the Conserved Stalk Domain by Hyperglycosylation of the Globular Head Domain. *J Virol* **88**, 699–704 (2014).

63. Hai, R. *et al.* Influenza viruses expressing chimeric hemagglutinins: globular head and stalk domains derived from different subtypes. *Journal of Virology* **86**, 5774–5781 (2012).

64. Veneziano, R. *et al.* Role of nanoscale antigen organization on B-cell activation probed using DNA origami. *Nat. Nanotechnol.* **15**, 716–723 (2020).

65. Kraft, J. C. *et al.* Antigen- and scaffold-specific antibody responses to protein nanoparticle immunogens. *Cell Reports Medicine* 100780 (2022) doi:10.1016/j.xcrm.2022.100780.

66. Chaudhary, N., Weissman, D. & Whitehead, K. A. mRNA vaccines for infectious diseases: principles, delivery and clinical translation. *Nat. Rev. Drug Discov.* **20**, 817–838 (2021).

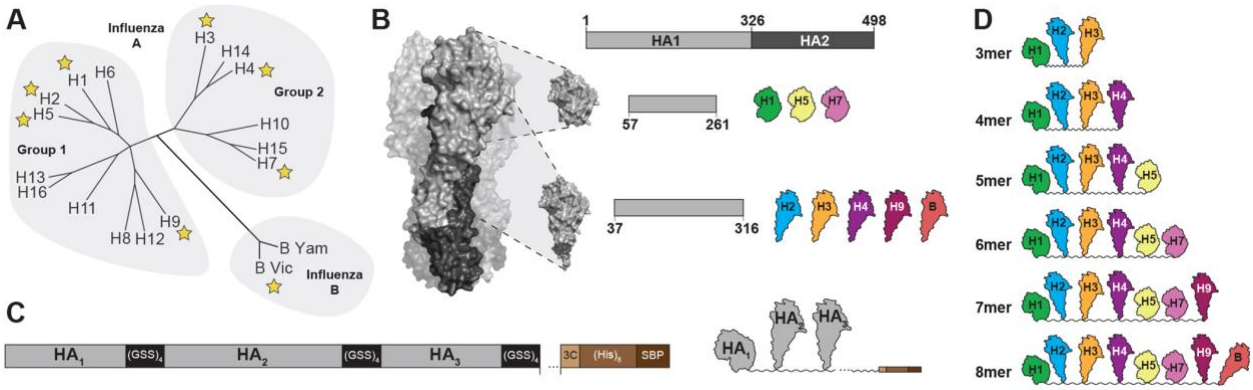

Figure 1: Design of Beads-on-a-string (BOAS) immunogens- (A) Phylogenic tree of influenza hemagglutinin (HA) subtypes. Subtypes are further categorized as group 1, group 2 or influenza B, and stars indicate subtypes included in the BOAS. **(B)** Native trimeric HA structure (A/H3/Hong Kong/1968; PDB: 4FNK) is shown on the left, with the HA1 domain in light grey, and HA2 in dark grey. A construct diagram of full-length HA is shown at the top with the locations of head domain segments within HA1. Head domains of H1, H3, and H7 span residues 57-261, and head domains of H2, H3, H4, H9, and B span 37-316 of the HA1 region of HA. **(C)** Construct diagram of HA BOAS. BOAS are assembled by linking HA head domains (light grey) into a single polypeptide chain where HA head domains are separated by a flexible linker with 4 (GSS) repeats. The C-terminus consists of an HRV-3C protease cleavable His tag and streptavidin-binding-protein (SBP) tag for purification and other affinity tags. **(D)** BOAS used in this study.

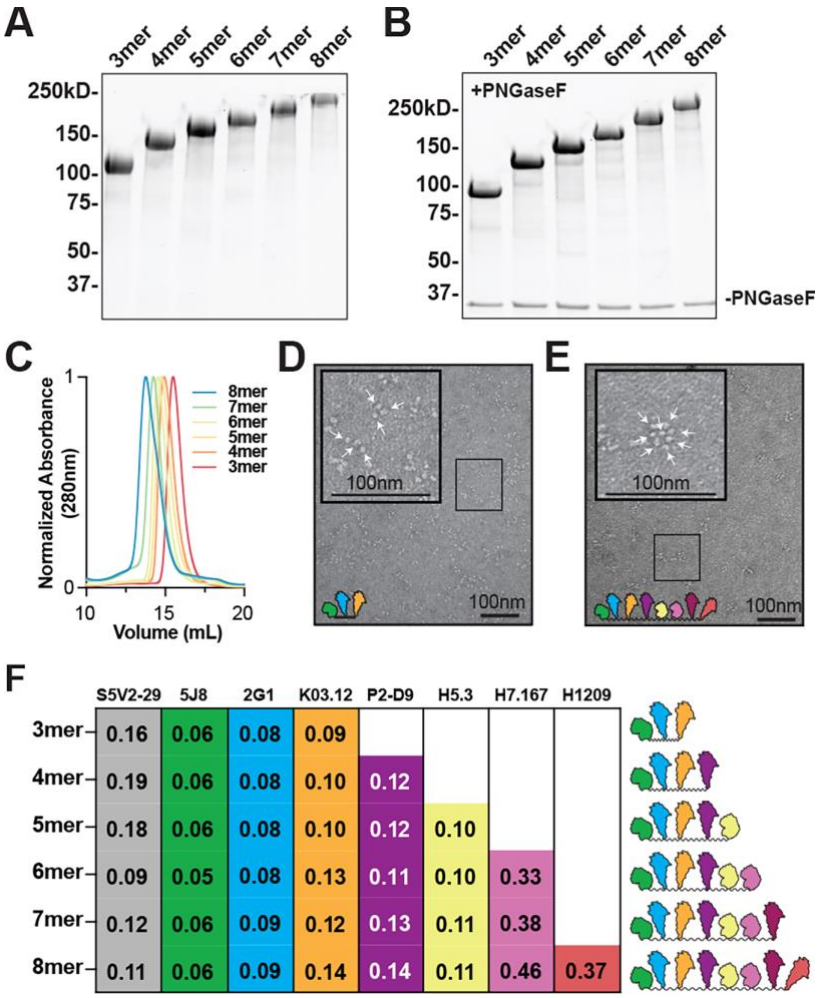

Figure 2: Biochemical Characterization of BOAS- A) SDS-PAGE analysis of 3mer-8mer BOAS under non-reducing conditions. **B)** SDS-PAGE analysis of 3mer-8mer BOAS under non-reducing conditions following glycan digestion with PNGase-F. **C)** Size exclusion chromatography traces of 3mer-8mer BOAS on an Superdex 200 column in PBS. **D)** Negative stain electron microscopy (NS-EM) images of the 3mer. Arrows point to individual HA monomers. Inset image is 2.5X zoomed enlarged image of boxed area. **E)** Negative stain electron microscopy (NS-EM) images of the 8mer. Arrows point to individual HA monomers. Inset image is 2.5X zoomed enlarged image of boxed area. **F)** Characterization via ELISA of BOAS components with subtype-specific antibodies. K_D values in µM are reported for each antibody for each BOAS immunogen. Antibodies corresponding to each component are as follows: S5V2-29 (interface, all components except B/Mal/04), 5J8 (RBS, H1), 2G1 (RBS, H2), 3E5 (RBS, H3), P2-D9 (H4), H5.3 (RBS, H5), H7.167 (RBS, H7), H1209 (RBS, B).

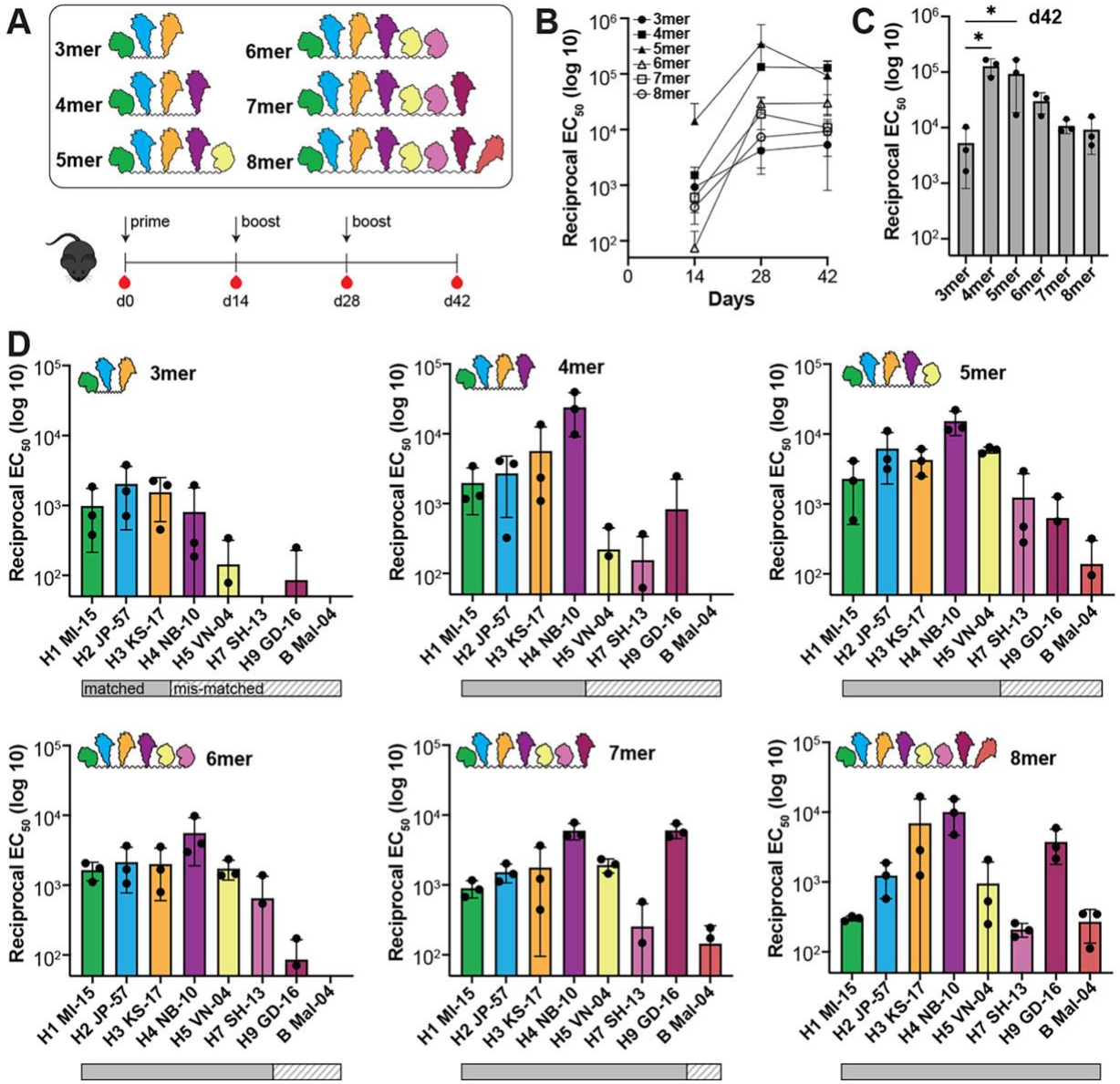

Figure 3: Murine immunizations with 3mer-8mer BOAS- A) Schematic of immunization regimen with 3mer-8mer BOAS. Mice were primed with 20µg of BOAS, followed by two homologous boosts two weeks apart. **B)** Immunogenicity of BOAS over time as determined by serum ELISA. Serum reactivity to each immunogen is reported as the reciprocal of the EC_{50} dilution factor for each group (n=3) and d14, d28, and d42. Data points are an average of n=3 mice and error bars are +/- 1 s.d. **C)** Serum titers to each BOAS at the final time point, d42. Data points for single time point antigen titers are from individual mice (n=3), bars represent mean titers and error bars are +/- 1 s.d., * = $p<0.05$ as determined by Kruskal-Wallis test relative to 3mer. **D)**

Serum titers to full-length HA trimers elicited by 3mer-8mer BOAS. Solid bars below each plot indicate a matched sub-type, and striped bars indicate a mis-matched subtype (i.e. not present in the BOAS).

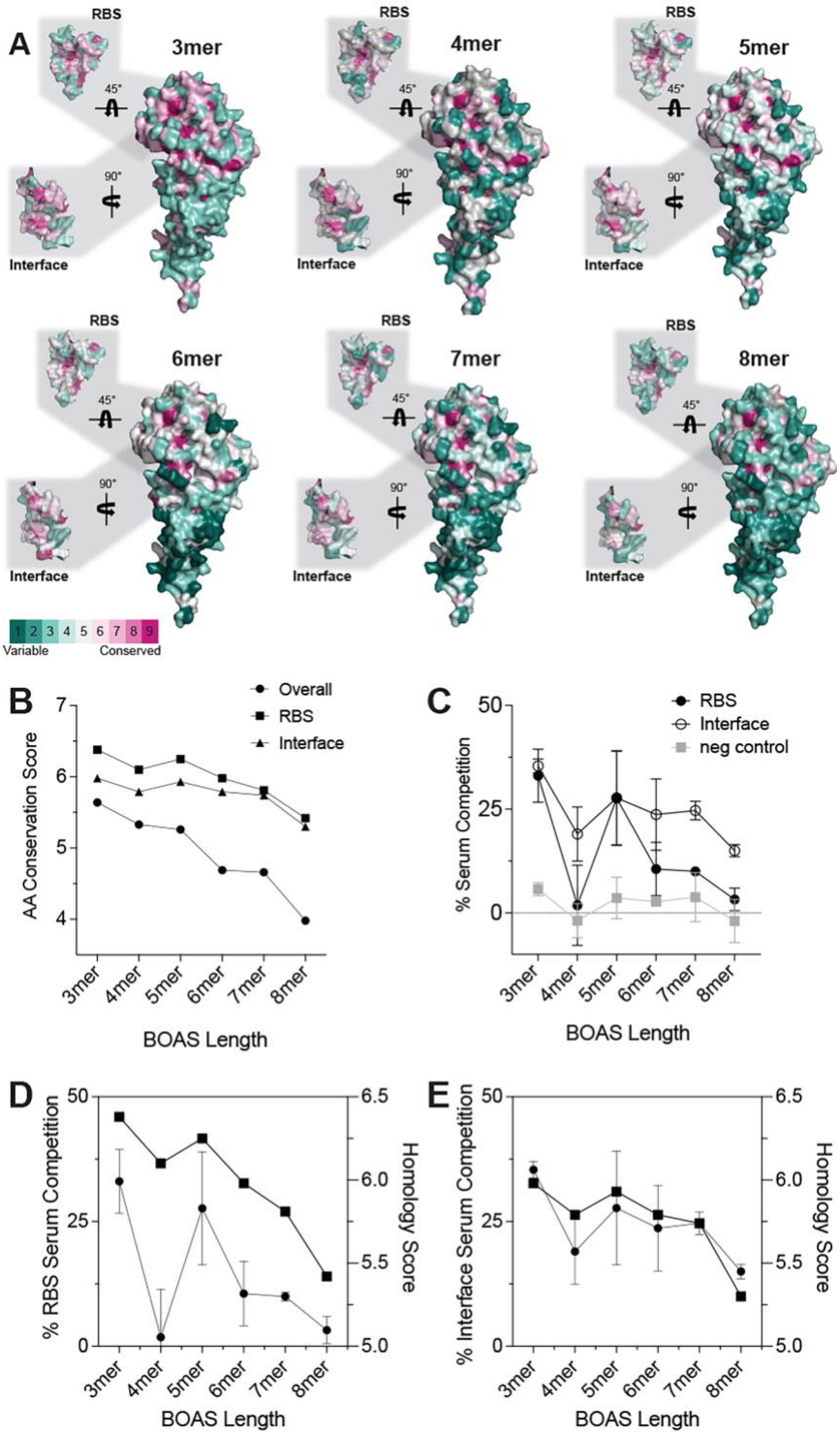

Figure 4: BOAS component epitope homology and serum competition A) Amino acid conservation of each BOAS projected on the A/H2/Japan/1957 head domain structure (PDB: 2WRE). Variability and conservation scores were determined as the % conservation of each

residue at each position for each BOAS composition. Cut-outs are RBS and Interface epitopes with their respective conservation. **B)** Homology score as determined by the average % conservation of each residue across the entire protein sequence (overall, circle), and the RBS (square) and interface (triangle) epitopes. **C)** Serum competition to RBS and interface epitopes as determined via competition with a cocktail of RBS-directed antibodies, interface-directed antibodies, or a stem-directed negative control antibody. % competition is determined by the relative decrease in serum binding to each BOAS normalized to an untreated control. Each data point represents a mean from n=3 mice and error bars are +/- 1 s.d. **D)** Trend overlay of % serum competition with RBS-directed antibodies and homology score of the RBS epitope as a function of BOAS length. **E)** Trend overlay of % serum competition with interface-directed antibodies and homology score of the interface epitope as a function of BOAS length.

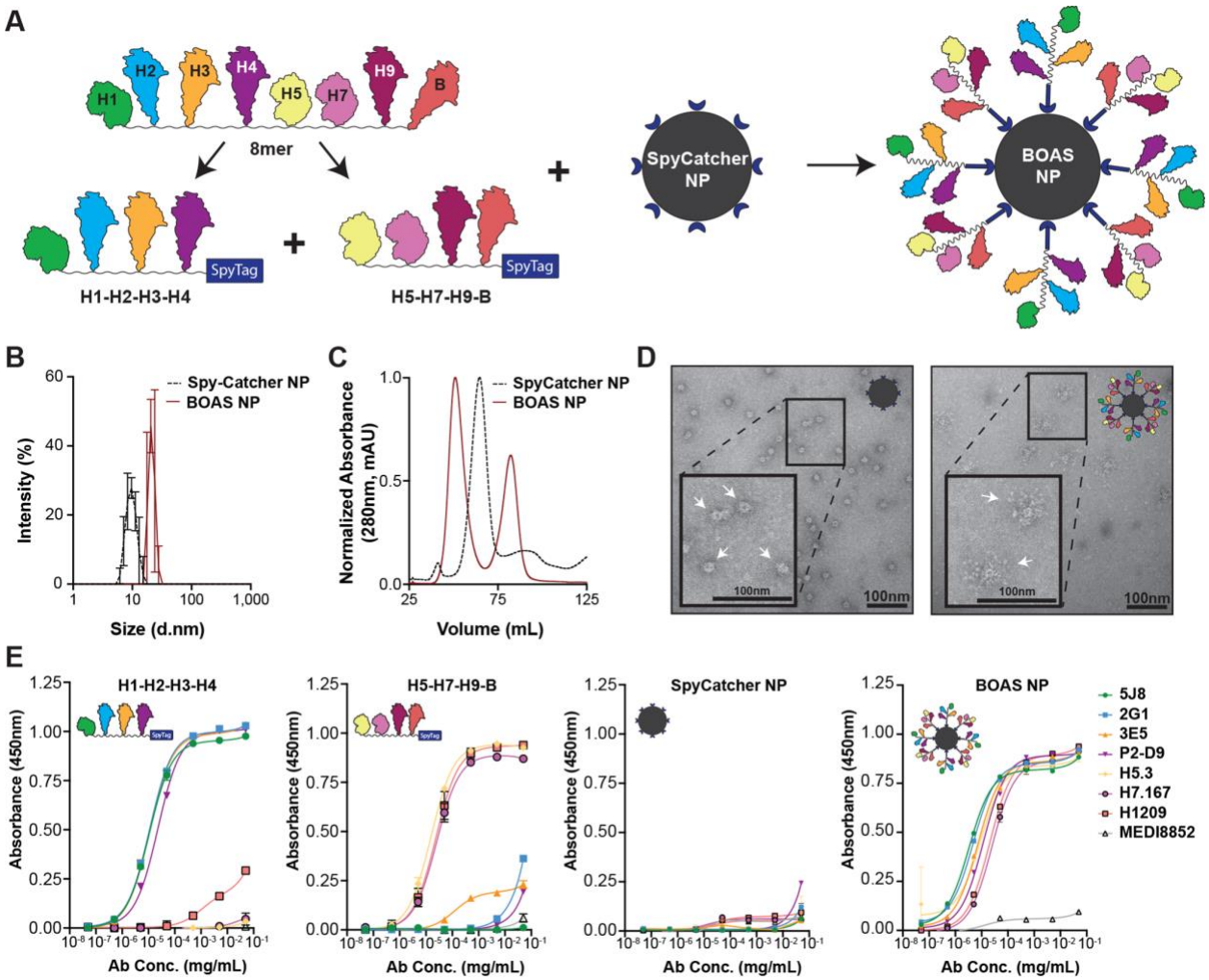

Figure 5: Design of BOAS nanoparticle (NP) immunogens- A) Schematic of design of BOAS nanoparticles. The eight original 8mer components were split into two 4mers, the first containing H1, H2, H3, and H4 (H1-H2-H3-H4), and the second containing H5, H7, H9, and B (H5-H7-H9-B). Each were expressed with an N-terminal SpyTag, then attached at equal molar ratios to an N-terminally fused SpyCatcher ferritin nanoparticle (SpyCatcher NP). This yields a ferritin nanoparticle with both 4mer BOAS conjugated to its surface (2x4mer BOAS NP). **B)** Dynamic light scattering (DLS) distributions of SpyCatcher NP and 2x4mer BOAS NP. Curves represent an average of 3 technical replicate measurements and error bars are +/- 1 s.d. **C)** Size exclusion traces of SpyCatcher NP and 2x4mer BOAS NP on an S400 column. **D)** Representative NS-EM image of SpyCatcher NP. Arrows indicate individual nanoparticles, and the inset is a 2X zoom of the boxed area. Representative NS-EM image of BOAS NP. Arrows indicate individual

nanoparticles, and the inset is a 2X zoom of the boxed area. **E)** ELISA of BOAS components, SpyCatcher NP, and 2x4mer BOAS NP with structure-dependent subtype-specific antibodies and a negative control stem-directed antibody, MEDI8852. ELISA data points are technical duplicates and error bars are +/- 1 s.d.

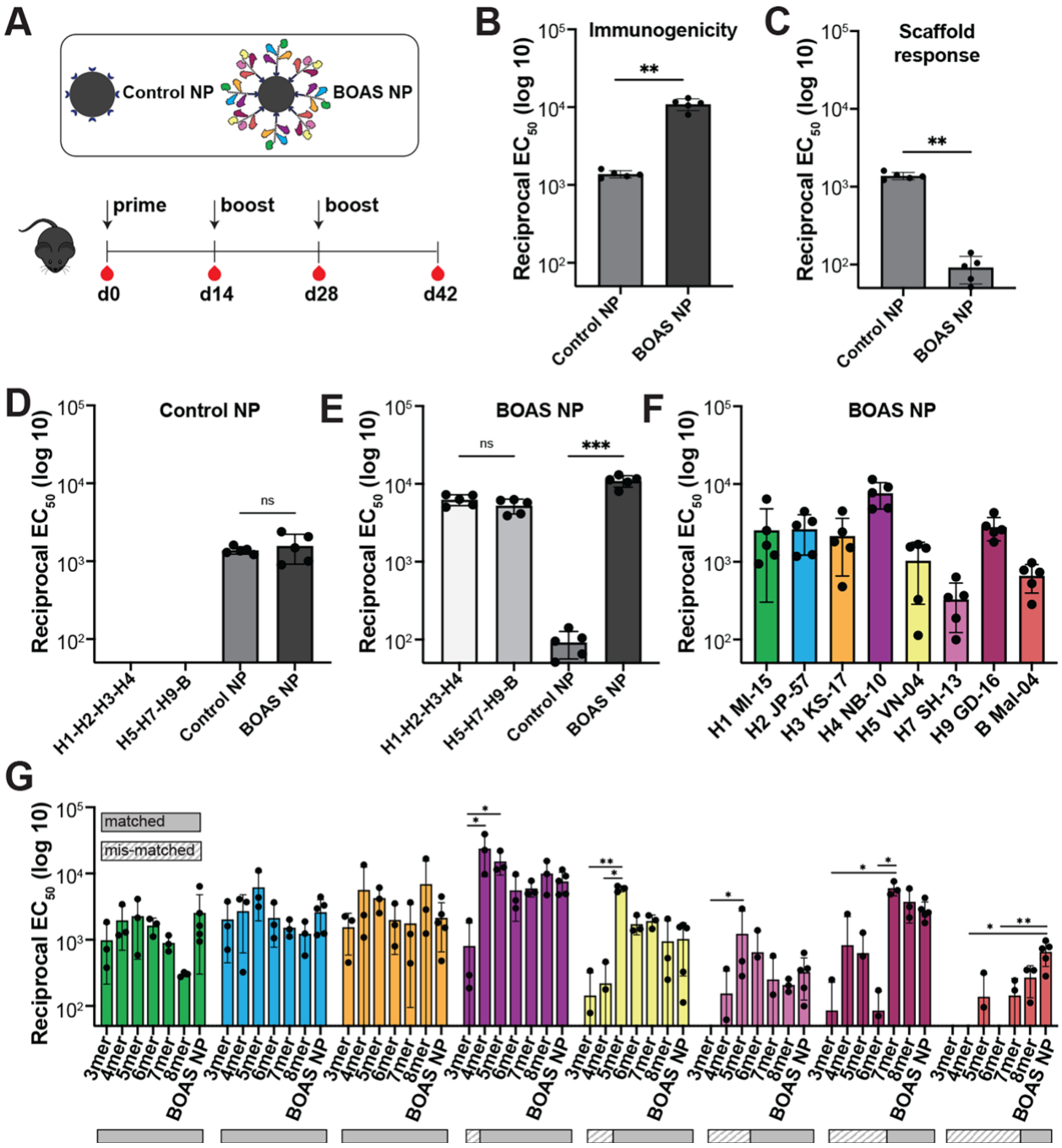

Figure 6: Murine Immunizations with BOAS NP A) Schematic of immunization regimen with 2x4mer BOAS NP and SpyCatcher NP control. Mice were primed with 20µg of NP, followed by two homologous boosts two weeks apart. **B)** Serum reactivity to each immunizing antigen at d42. ** $p<0.01$ as determined by Mann-Whitney test. **C)** Serum reactivity to Control NP scaffold by

both groups. ** $p<0.01$ as determined by Mann-Whitney test. **D)** Serum reactivity elicited by Control NP group (n=5) at d42 to both individual BOAS components (H1-H2-H3-H4 and H5-H7-H9-B), Control NP, and BOAS NP. n.s. = not significant ($p>0.05$) as determined by Kruskal-Wallis test. **E)** Serum reactivity elicited by BOAS NP group (n=5) at d42 to both individual BOAS components (H1-H2-H3-H4 and H5-H7-H9-B), Control NP, and BOAS NP. *** $p < 0.001$ and n.s. = not significant ($p>0.05$) as determined by Kruskal-Wallis test. **F)** Serum reactivity elicited by BOAS NP group (n=5) to individual full-length HA components of BOAS at d42. **G)** Serum reactivity to each individual full-length HA component of BOAS (H1 green, H2 blue, H3 orange, H4 purple, H5 yellow, H7 pink, H9 maroon, B salmon) by 3mer-8mer BOAS and BOAS NP. Solid bars below each plot indicate a matched sub-type, and striped bars indicate a mis-matched subtype (i.e. not present in the BOAS or NP). * $p<0.05$ and ** $p<0.01$ as determined by Kruskal-Wallis test with multiple comparisons. In all plots, data points for single time point antigen titers are from individual mice (n=5 for NP studies, n=3 for 3mer-8mer BOAS studies), bars represent mean titers and error bars are +/- 1 s.d.

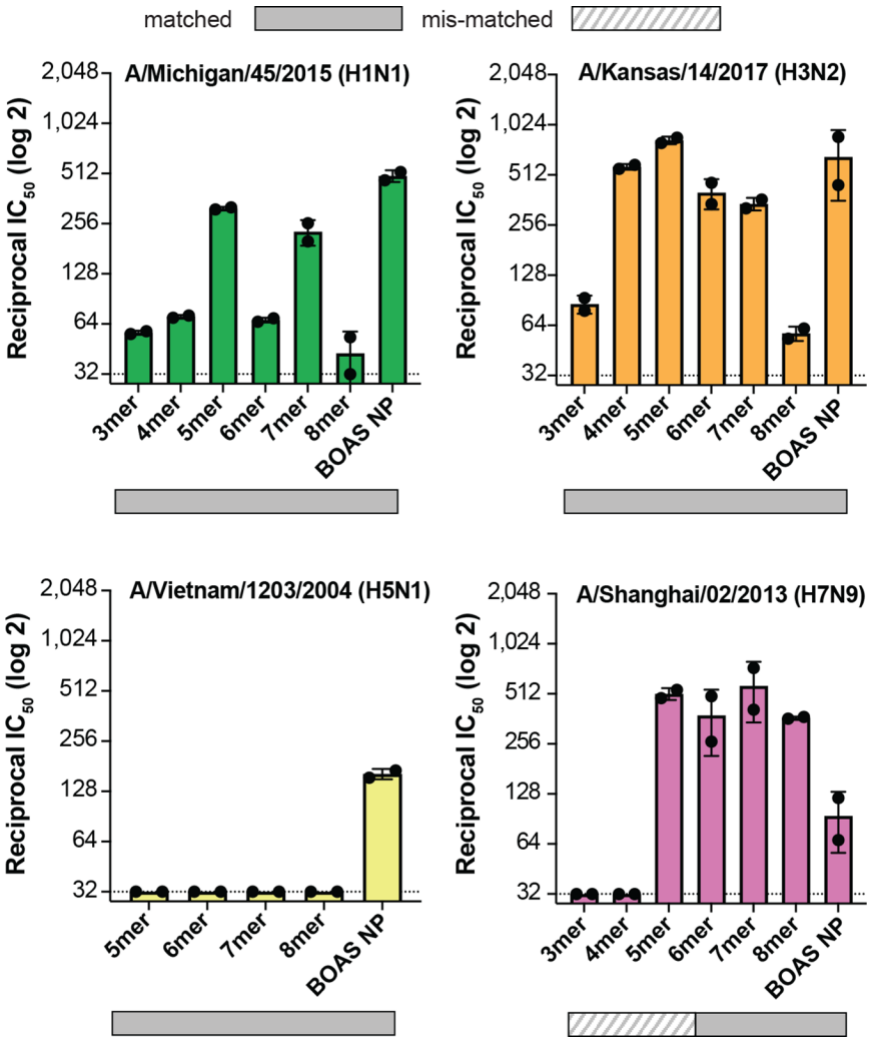

Figure 7: Microneutralization titers to matched and mis-matched virus- Microneutralization of matched and mis-matched psuedoviruses: H1N1 (green, top left), H3N2 (orange, top right), H5N1 (yellow, bottom left), and H7N9 viruses (pink, bottom right) with d42 serum. H1N1 and H3N2 and H5N1 viruses match components in all BOAS constructs tested and BOAS NP. The H7 component is present and matched in 6mer-8mer and BOAS NP and mismatched in 3mer-5mer. Dashed lines represent the first serum dilution (1:32), and points at the dashed line indicate IC50s at or below the limit of detection. Serum samples are pooled from n=3 (BOAS) or n=5 (BOAS NP) mice and individual data points are technical duplicates. The mean is denoted by a bar +/- 1 s.d.